AFRL-VS-HA-TR-2006-1145

Laboratory Experiments of Whistler Wave Interactions with Energetic Electrons

R. L. Stenzel
J. M. Urrutia

University of California
Department of Physics and Astronomy
Los Angeles, CA 90095-1547

Scientific Report No. 1

25 July 2006

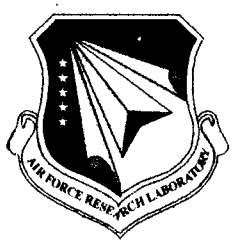

AIR FORCE RESEARCH LABORATORY
Space Vehicles Directorate
29 Randolph Road
AIR FORCE MATERIEL COMMAND
Hanscom AFB, MA 01731-3010

NOTICE AND SIGNATURE PAGE

Using Government drawings, specifications, or other data included in this document for any purpose other than Government procurement does not in any way obligate the U.S. Government. The fact that the Government formulated or supplied the drawings, specifications, or other data does not license the holder or any other person or corporation; or convey any rights or permission to manufacture, use, or sell any patented invention that may relate to them.

This report was cleared for public release and is available to the general public, including foreign nationals. Qualified requestors may obtain additional copies from the Defense Technical Information Center (DTIC) (http://www.dtic.mil). All others should apply to the National Technical Information Service.

AFRL-VS-HA-TR-2006-1145 HAS BEEN REVIEWED AND IS APPROVED FOR PUBLICATION IN ACCORDANCE WITH ASSIGNED DISTRIBUTION STATEMENT.

//Signature//	//Signature//
THOMAS R. HEINE, 1Lt Contract Manager	JOEL MOZER, Chief Space Weather Center of Excellence

This report is published in the interest of scientific and technical information exchange, and its publication does not constitute the Government's approval or disapproval of its ideas or findings.

REPORT DOCUMENTATION PAGE

Form Approved
OMB No. 0704-0188

1. REPORT DATE *(DD-MM-YYYY)*	2. REPORT TYPE	3. DATES COVERED *(From - To)*
25 July 2006	Scientific Report No. 1	July 2005 - July 2006

4. TITLE AND SUBTITLE
Laboratory Experiments on Whistler Wave Interactions with Energetic Electrons

5a. CONTRACT NUMBER
FA8718-05-C-0072

5b. GRANT NUMBER

5c. PROGRAM ELEMENT NUMBER
63287E

6. AUTHOR(S)
R.L. Stenzel and J.M. Urrutia

5d. PROJECT NUMBER
DARP

5e. TASK NUMBER
RR

5f. WORK UNIT NUMBER
59

7. PERFORMING ORGANIZATION NAME(S) AND ADDRESS(ES)

University of California
Department of Physics and Astronomy
Los Angeles, CA 90095-1547

8. PERFORMING ORGANIZATION REPORT NUMBER
444025-ST-25304

9. SPONSORING / MONITORING AGENCY NAME(S) AND ADDRESS(ES)
Air Force Research Laboratory
29 Randolph Road
Hanscom AFB, MA 01731-3010

10. SPONSOR/MONITOR'S ACRONYM(S)
AFRL/VSBXR

11. SPONSOR/MONITOR'S REPORT NUMBER(S)
AFRL-VS-HA-TR-2006-1145

12. DISTRIBUTION / AVAILABILITY STATEMENT
Approved for public release; distribution unlimited.

13. SUPPLEMENTARY NOTES

14. ABSTRACT
Whistler wave excitation in plasmas has been modeled in a laboratory experiment. The most efficient coupling is achieved with magnetic loop antennas which can deposit 50% of the applied energy into waves in a dense plasma with low ambient magnetic field. Since space plasmas are dilute, it is suggested to eject an expanding plasma plume into space for efficient wave excitation with a small magnetic antenna. The ejected waves have magnetic fields exceeding the ambient field. The properties of such nonlinear whistler modes have been investigated. Their propagation speed depends on amplitude and field topology, they can steepen into whistler shocks and strongly accelerate electrons. In the presence of neutrals, the energetic electrons produce visible light emission. Anisotropic electron distributions are formed which create whistler instabilities and emissions at different frequencies than applied. Scattering of electrons in phase space is evident.

15. SUBJECT TERMS
Whistler waves, Nonlinear phenomena, Electron scattering

16. SECURITY CLASSIFICATION OF:			17. LIMITATION OF ABSTRACT	18. NUMBER OF PAGES	19a. NAME OF RESPONSIBLE PERSON
a. REPORT	b. ABSTRACT	c. THIS PAGE			Thomas R. Heine, 1Lt
Unclassified	Unclassified	Unclassified	UU	16	19b. TELEPHONE NUMBER *(Include area code)*

TABLE OF CONTENTS

FIGURES

FIGURES (Continued)

1. SUMMARY

The research deals with excitation of large-amplitude whistler waves into a magnetized laboratory plasma. Magnetic loop antennas are used since they couple better to the wave magnetic field than electric dipoles do to the electric field. Whistler-mode waves with wave magnetic field exceeding the background magnetic field are produced. In one configuration, the net magnetic field has the topology of a field-reversed configuration (FRC). The FRC splits into two oppositely propagating wave packets which self-consistently develop twisted field lines as in a spheromak. The properties of such nonlinear fields are studied. The wave packets contract with increasing amplitude which characterizes them as whistler solitons. However, the collision between whistler solitons is different from those of electrostatic waves: The solitons collide inelastically and dissipate their energy in electron heat and light radiation. Detailed observations also show that higher frequency magnetic oscillations are excited by a whistler spheromak. These spontaneous oscillations are possibly created by a kinetic whistler instability associated with anisotropic electron heating ($T_{\rm perp} > T_{\|}$ or parallel electron beams).

2. DETAILED FINDINGS

2.1. Overview

We briefly review the setup of our laboratory experiments, the measurement methods and basic properties of the waves excited. Then we describe wave-wave and wave-particle interactions. The former involves the study of wave collisions, the latter electron energization by nonlinear whistlers.

2.2. Review of Experimental Setup

Our experiments are performed in a large (1 m diam, 2.5 m length) pulsed dc discharge plasma generated with a 1 m diam oxide-coated cathode shown schematically in Fig. 1(a).

The parameter regime ($n_e \simeq 10^{12}$ cm^{-3}, $kT_e \simeq 2$ eV, $B_0 = 5$ G) is that described by electron magnetohydrodynamics (EMHD, magnetized electrons, unmagnetized ions). Insulated magnetic loop antennas (2-4 turns, 10-30 cm diam) are inserted into the plasma center and a charged (1200 V) capacitor (0.1-10 μF) is discharged into the loop using a fast, high power transistor. This results

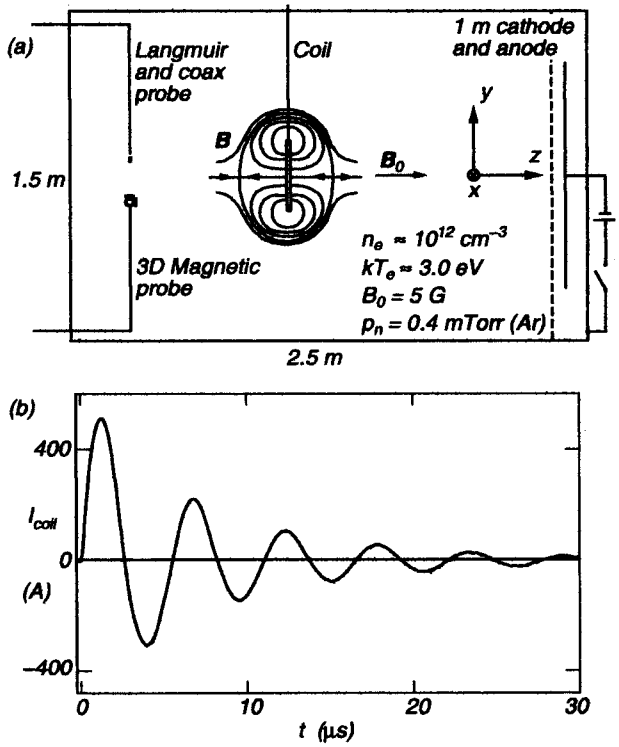

FIG. 1 (a) Schematic of the experimental setup and relevant parameters. (b) Typical waveform of the coil current expressed in Ampere-turns.

in a damped oscillatory current ($I_{\rm max} \simeq$ 100-300 A, which decays with period $T = 2\pi(LC)^{1/2} \simeq$ 2-25 μs. From the decay time and the L-C circuit elements, the series resistance, hence power dissipated in the circuit, can be determined. Of particular interest is the increase in absorbed power in plasma vs that in vacuum. Typical values show that 50% of the applied power of $P = I_{\rm peak}V_{\rm peak}/2 \simeq$ 100 kW can be deposited into the the plasma.

In vacuum, the magnetic field in the center of the loop at the peak current can be as large as $B = 100$ G $\gg B_0 = 7$ G. Figure 1(b) shows the typical ringing waveform of the antenna current. The local magnetic field is measured with a single magnetic probe containing three orthogonal small loops (5 mm diam) which can be moved in three orthogonal directions. From highly repeatable ($\delta n/n < 3\%$) discharges at a fast repetition rate (1 Hz) the space-time dependence of the field is measured with a four-channel digital oscilloscope (8 bit, 0.2 ns resolution, LeCroy 6200), stored and digitally processed. At

each probe position, we measure the fields in vacuum and in plasma with different current polarity. This allows us to distinguish the fields created by plasma currents, $\mathbf{B}_{\rm plasma}$, from those created by antenna currents, $\mathbf{B}_{\rm coil}$, and to demonstrate important differences in the axial field direction relative to $\mathbf{B}_0$. A Langmuir probe is also attached next to the magnetic probe so as to measure the plasma parameters in space and time. We also perform light emission measurements with a photomultiplier tube with good temporal (< 0.1 μs) and spatial (< 2 cm $\perp$ line of sight) resolution.

2.3. Experimental Results

2.3.1. Magnetic Topologies

When a rising magnetic field is applied with a loop antenna in a plasma, an opposing magnetic field is created by induced plasma currents. In the EMHD parameter regime, the induced field propagates in the whistler mode away from the antenna such that the antenna vacuum field penetrates into the plasma at a whistler transit time. During the turn-on of a loop field directed opposite to the ambient field a whistler wave with wave field along the ambient field is excited. We call this mode a whistler mirror since it compresses the field lines in the center of the wave packet. A measurement example is shown in Fig. 2.

It displays contours of the total axial magnetic field. To the right and left of the coil ($z = 0$) are yellow contours with peak magnetic field of 17 G compared to the ambient field of 5 G. These are the large amplitude whistler mirrors. After the whistler mirrors propagate away, the field near the antenna is close to the potential

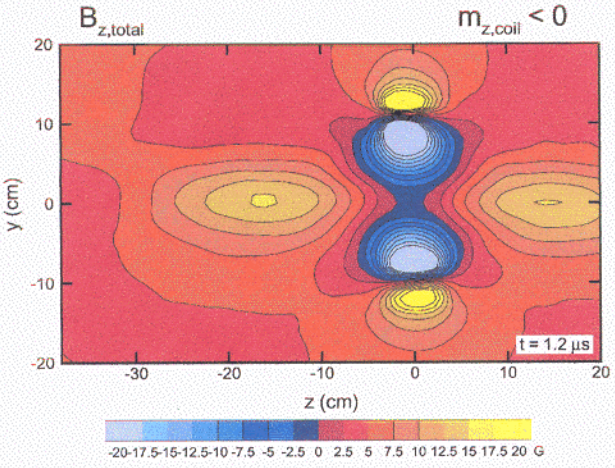

FIG. 2 Contours of the net ($\mathbf{B}_{\rm tot} = \mathbf{B}_0 + \mathbf{B}_{\rm coil} + \mathbf{B}_{\rm plasma}$) axial magnetic field component. The coil , located at z=0, creates a field reversal. During the current rise an opposing field with $\mathbf{B}_{\rm wave}||\mathbf{B}_0$ is induced which propagates away as two whistler wave packets (yellow peaks on axis).

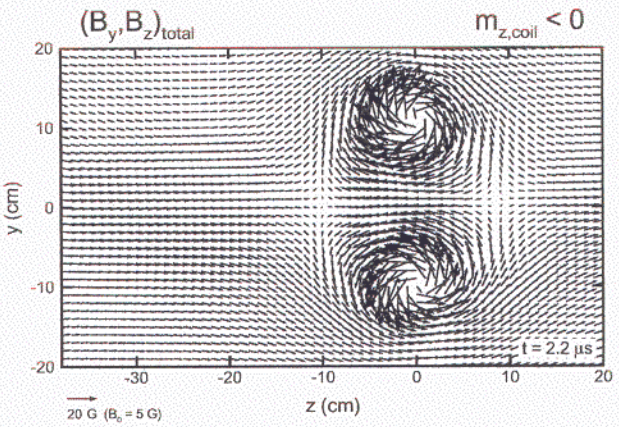

FIG. 3 Vector field ($\mathbf{B}_y, \mathbf{B}_z$) at the time of the peak antenna current. The shielding field has propagated away in the whistler mode and the vacuum antenna field has penetrated into the plasma forming a FRC.

field in vacuum. Figure 3 shows a measured vector field when the coil current reaches a maximum.

When the coil current decays, plasma currents are induced which try to maintain the FRC. They flow in the vicinity of the antenna across magnetic field, thus are electron Hall currents. A critical moment arises when the coil current goes through zero and the antenna field reverses sign: As schematically shown in Fig. 4 two X-type null points are formed above and below the coil.

For axial symmetry, they have a toroidal separator. At these magnetic nulls, field lines around the coil reconnect with field lines inside the FRC separatrix to form new field lines around the two plasma current rings. This flux addition enhances the induced currents. With increasing coil current, the null points move radially away from the coil. When the inner null point reaches the axis, all the closed field lines of the original FRC have been reconnected. As schematically shown in Fig. 5, the inner null line degenerates into a 3-D null point.

Topologically, it is called a "degenerate radial null," meaning that it joins two separatrix surfaces or exhibits

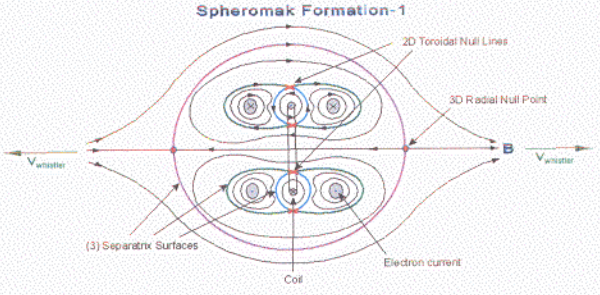

FIG. 4 Schematic field line picture showing how reconnection at two magnetic null lines forms two spheromaks from a single FRC.

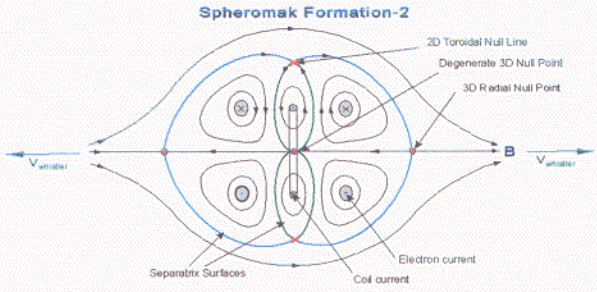

FIG. 5 Schematic field line picture showing an intermediate stage of spheromak formation. The inner null line has formed a degenerate 3-D null point on axis. it is topologically unstable and splits into two regular 3-D radial nulls shown in Fig. 6.

two different fans. A degenerate null point is not stable and changes immediately into two ordinary radial null points, shown schematically in Fig. 6.

Now two spheromaks have been formed, each with two radial nulls on axis. The O-type null in the toroidal current layer is actually not a magnetic null since the spheromak self-consistently develops a toroidal magnetic field $B_{\rm tor}$. The reason is that the toroidal electron fluid flow twists the frozen-in field lines. The toroidal twist between the two spheromaks implies opposite signs of $B_{\rm tor}$ in each spheromak. The spheromak propagating along $\mathbf{B}_0$ has always a right handed twist or positive helicity, while the spheromak propagating against $\mathbf{B}_0$ has negative helicity. A measurement of the two spheromaks is shown in Fig. 7 which displays for clarity only the axial magnetic field component. The blue contours of negative B_z are the two whistler spheromaks which propagate away from the antenna.

2.3.2. Nonlinear Propagation

The propagation speed of whistler spheromaks and mirrors differs from that of linear whistlers. From time-of-flight measurements at different wave amplitudes we

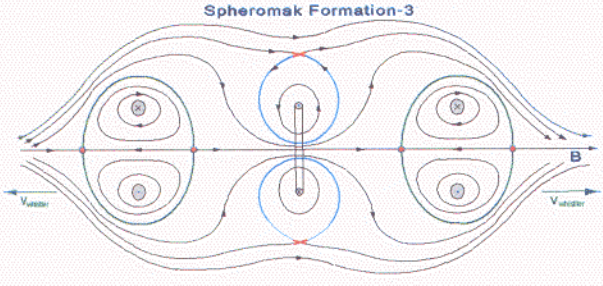

FIG. 6 Final stage of spheromak formation. The two outward propagating whistler spheromaks are separated by a whistler mirror.

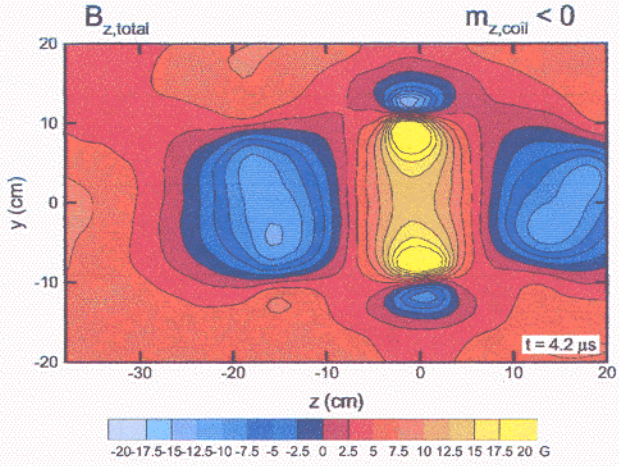

FIG. 7 Contours of the net axial magnetic field component when two whistler spheromaks (blue contours=field reversals) have been excited by the coil at $z = 0$.

have measured the nonlinear propagation characteristics and displayed the result in Fig. 8. Whistler mirrors propagate faster and whistler spheromaks propagate slower than linear whistler modes.

This result is qualitatively understood since the group and phase velocity of linear whistlers scales as the square root of the ambient magnetic field. The mirror enhances the net field, hence propagates faster. The reverse holds true for the spheromak. However, this picture is only globally correct. Locally, the whistler spheromak should stagnate at its null point, but this is not the case. However, it does steepen into a narrower structure than a linear wave. Figure 9 shows the widths of the wave packets vs wave magnetic field.

With increasing amplitude the whistler spheromak contracts along the direction of wave propagation while the mirror stretches. Accompanied with the contraction of the spheromak is a relative increase in the wave am-

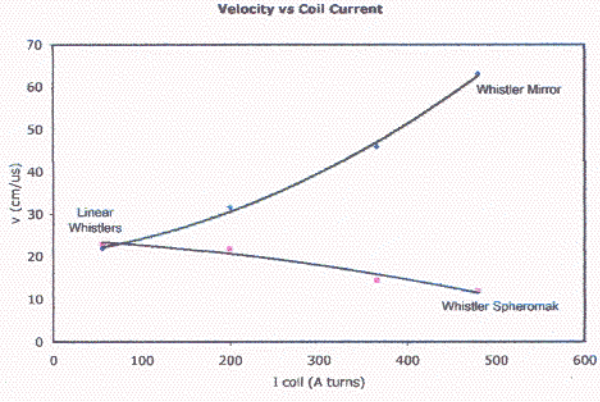

FIG. 8 Propagation speed of whistler spheromaks and mirrors vs wave amplitude.

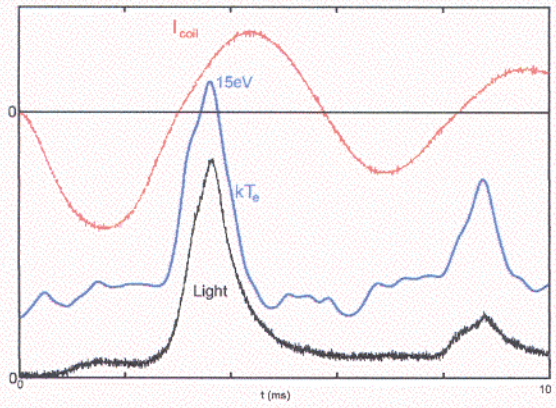

FIG. 12 Light emission (black) and electron bulk temperature (blue) vs time. Comparison with the antenna current waveform (red) shows strong electron heating only when whistler spheromaks are excited.

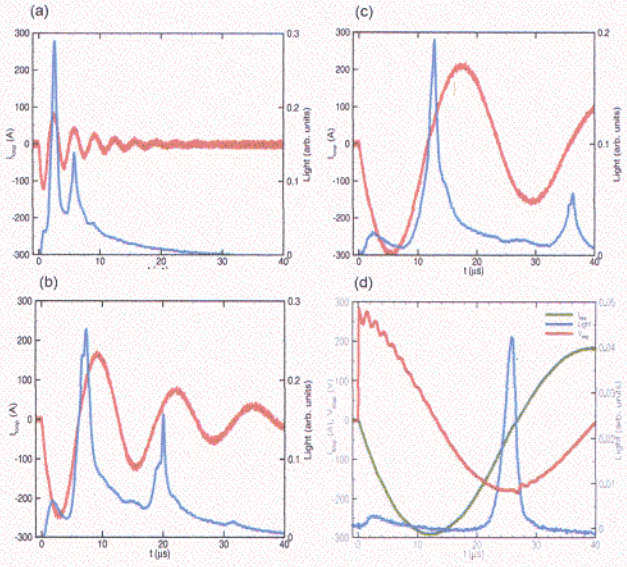

FIG. 13 Waveforms of the oscillatory antenna current and the spiky light emission for different rf periods. The light pulse is observed 20 cm axially away from the antenna. It occurs only during spheromak emission and its duration is nearly independent of rf period. (d) shows that both antenna voltage (red) and current (green) exhibit loading effects when the electrons are heated.

The duration of electron energization is given by the transit time of the spheromak across the probe or optical path (2 cm axial resolution). Without electron confinement, there is little electron heat remaining in the wake of the spheromak.

Figure 13 shows how the duration of the spheromak or light pulse varies with applied frequency. Surprisingly, the half-width of the light pulse remains of order 1-2 μs as the rf period is varied from 4 μs [Fig. 13(a)] to 50 μs [Fig. 13(d)]. Unlike a linear wave, the axial length of the spheromak is not determined by the rf period but by the shorter radial transit time of the magnetic null line from the coil radius to the coil center.

Attempts have been made to image the light emission with a high-speed camera. Figure 14 gives an example of a picture of the coil taken with a Canon EOS-1DS camera. In spite of a fast shutter time (1/8000 sec) the spheromak light pulse is time averaged hence only a broad glow in the antenna region is visible. A blue glow appears near the antenna wire.

Radial profiles of the light intensity have been measured with the photomultiplier which has provides full time resolution ($\lesssim 0.1$ μs). Figure 15 displays light intensity traces vs radius at different times after spheromak formation. The light starts near the antenna wire, propagates within $\lesssim 1$ μs radially inward to fill the entire coil interior. Since during the phase of spheromak creation an X-type magnetic null line also propagates radially inward the initial electron acceleration is thought to occur in the magnetic null line.

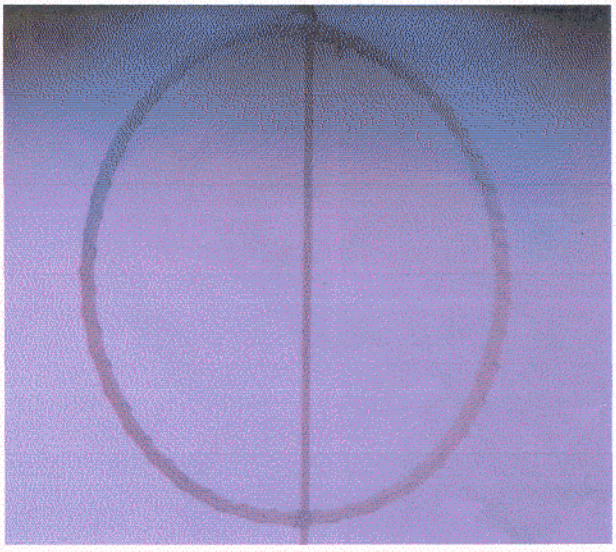

FIG. 14 Digital picture of the antenna region during pulse excitation. The afterglow plasma is dark and the light is due to emission of whistler spheromaks.

2.3.5. High Frequency Whistler Instability

Close inspection of the magnetic probe signal ($\propto$ dB/dt) shows that under certain conditions oscillations arise at a frequency much higher than the applied frequency. The oscillations occur in the frequency regime of 5-10 MHz and occur only during spheromak emission.

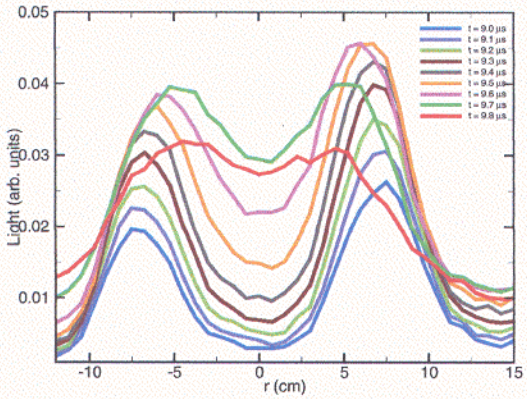

FIG. 15 Light emission vs radius at different times during spheromak formation. The light is radially resolved to within 2cm, axially averaged, but fully time-resolved ($\lesssim 0.1$ μs).

The oscillations arise in all field components. They exhibit shot-to-shot fluctuations but, in spite of some amplitude loss, they can be averaged so as to obtain the space-time dependence.

Figure 16 shows that the high-frequency magnetic oscillations propagate axially at a velocity $v_z \simeq 100$ cm/μs, which is much higher than that of the whistler spheromak ($\simeq 20$ cm/μs).

Figure 17 shows that the waves also propagate radially outward as seen from contour plots of orthogonal field components in the $y-z$ plane which exhibit oblique phase fronts. Typical wavelengths are 10-15 cm. Interference patterns are common. The orthogonal field components exhibit some delay indicating elliptical polarization.

The source for the high frequency magnetic waves has not yet been identified. Whistler instabilities due to anisotropic electron distributions are suspected since the oscillations are only seen under conditions of electron energization in whistler spheromaks. Further investigations will be performed to identify these wave-particle interactions.

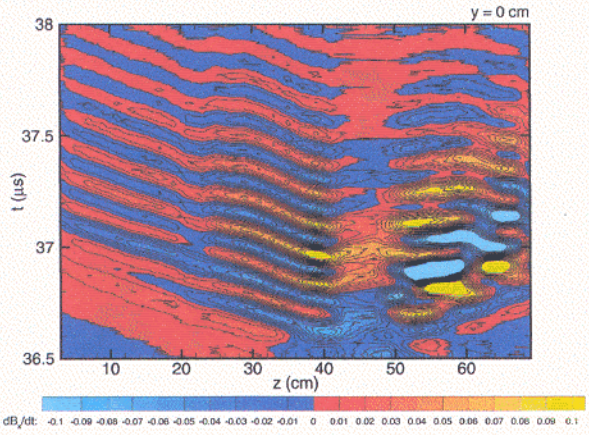

FIG. 16 Contour plot of dB_y/dt in the $z-t$ plane ($x = 0$) showing axial propagation of 7 MHz oscillations in a whistler spheromak. The antenna is located at 47.5 cm.

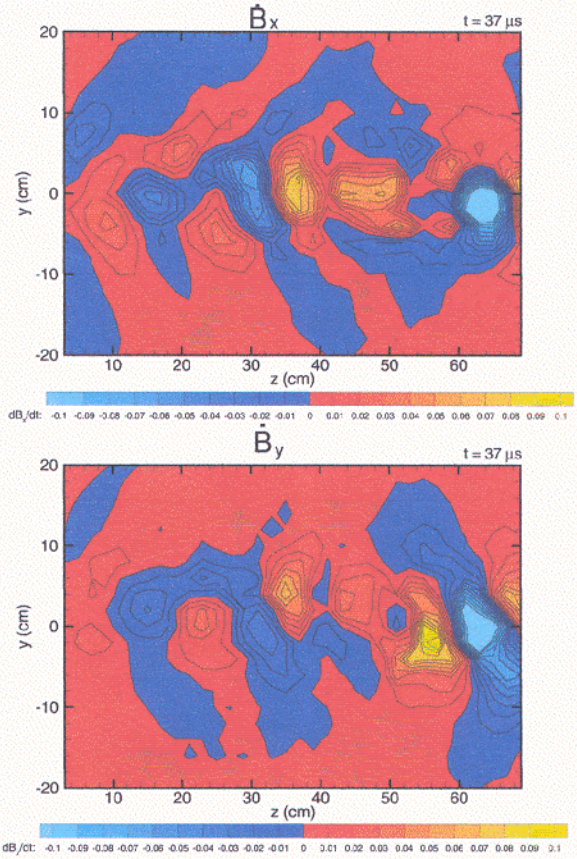

FIG. 17 Contour plot of dB_x/dt and dB_y/dt in the $y-z$ plane ($x = 0$) at a fixed time showing an interference pattern of obliqueley propagating 7 MHz oscillations in a whistler spheromak. The antenna is located at 47.5 cm.

3. CONCLUSIONS

In summary, we have shown experimental observations on the excitation of large amplitude whistler waves from magnetic antennas. Whistler modes with wave magnetic fields large compared to the ambient magnetic fields have been produced. Electrons are strongly accelerated in whistler spheromaks. Anisotropic distributions are produced which in turn produce secondary whistler instabilities. These are all evidence for wave-particle interactions in large amplitude whistlers.